

Velocity Analysis of Moving Objects in Earth Observation Satellite Images Using Multi-Spectral Push Broom Scanning

ERIC KETO¹ AND WESLEY ANDRÉS WATTERS²

¹*Harvard University, Institute for Theory and Computation
60 Garden Street, Cambridge, MA USA*

²*Wellesley College, Department of Physics and Astronomy
106 Central St., Wellesley, MA 02481, USA*

ABSTRACT

In this study, we present a method for detecting and analyzing the velocities of moving objects in Earth observation satellite images, specifically using data from Planet Labs’ push broom scanning satellites. By exploiting the sequential acquisition of multi-spectral images, we estimate the relative differences in acquisition times between spectral bands. This allows us to determine the velocities of moving objects, such as aircraft, even without precise timestamp information from the image archive. We validate our method by comparing the velocities of aircraft observed in satellite images with those reported by onboard ADS-B transponders. The results demonstrate the potential, despite challenges posed by proprietary data limitations, of a new, useful application of commercial satellite data originally intended as an ongoing, once-daily survey of single images covering the entire land-area of the Earth. Our approach extends the applicability of satellite survey imagery for dynamic object tracking and contributes to the broader use of commercial satellite data in scientific research.

Keywords: satellite imagery, Earth observations, data analysis, image processing, push broom scanning, aircraft velocities, ADS-B transponders, Planet Labs, multi-spectral images.

1. INTRODUCTION

In multi-spectral images made by satellites with push broom scanning, images in individual spectral bands are acquired sequentially in time and a moving object appears in a different location in the image of each spectral band. The velocity can be determined if the relative differences in the acquisition times are known for each spectral band. The effect is well known and analyzed in previous articles. This effect has been studied by [Etaya et al. \(2004\)](#) and [Easson et al. \(2010\)](#) with images from QuickBird satellites, and by [Heiselberg \(2019\)](#) and [Heiselberg & Heiselberg \(2021\)](#) with images from Sentinel-2 satellites.

The satellites of Planet Labs Corporation (PLC) use push broom scanning to survey most of the land area of the Earth with a daily revisit rate. Their archive of images, extending back several years, can be used to identify moving objects almost anywhere on Earth, although within a narrow time window of a few seconds per day. However, the acquisition times of the images in each spectral band are not available in the PLC archive. Only an approximate time is published for the set of images at each location. Without further assumptions this limits the determination of velocities to objects that move or change with a characteristic time scale of the revisit rate of one day. [Drouyer et al. \(2019\)](#) and [Chen et al. \(2021\)](#) have used PLC images to identify moving vehicles and estimate traffic densities but not vehicle velocities. Recently, [van Etten \(2024\)](#) proposed a method to estimate vehicle velocities with PLC images.

In a previous article ([Keto & Watters 2023](#)), we proposed a method to use information within the images to estimate differences in the acquisition times of images in different spectral bands to an accuracy of a few tens of milliseconds. This is sufficient to study objects moving at velocities of tens of m s^{-1} rather than tens of m day^{-1} with an accuracy in velocity that is limited by the positional accuracy of a few m pixel^{-1} in the PLC images. In [Keto & Watters \(2024\)](#) this procedure was followed to derive the altitudes of balloons from images made by PLC satellites. The balloons are good targets because of their large size, high brightness, and the velocities of the balloons are low enough to approximate as zero. In this article, we extend our analysis to trajectories of aircraft over a range of velocities of a few hundred m

s^{-1} . We verify our method by comparing the aircraft velocities measured from PLC images to the aircraft velocities reported from their onboard ADS-B transponders.

The commercialization of space presents new opportunities in the quantity and character of available data. PLC satellites have unique capabilities with higher spatial resolution (~ 4 m) and a more frequent revisit rate (daily) than the NASA Landsat or ESA Sentinel satellites (10 - 15 m resolution and revisit rates of several days). The scientific use of commercial data can be challenging if proprietary restrictions on information, performance and procedures results in omissions of data such as time, one of the fundamental properties of the universe along with space, energy and mass.

2. METHODS

2.1. *Design of the study*

The camera on the PLC SuperDove satellites covers eight spectral bands with a total field of view (FOV) of $\sim 35 \times 21$ km² and each spectral band covering one eighth the total FOV (Planet Labs Corporation 2021). With push broom scanning and a typical orbital altitude of 500 km, the satellites observe a region on the ground in all eight spectral bands within ~ 3.2 s. We assume that the camera operates asynchronously with the travel of the image footprint and with a constant rate over each image sufficient to obtain overlapping images in each spectral band. These smaller, single-band image strips, $\sim 35 \times 2.6$ km², are mosaiced by PLC into larger images with approximately the same size as the total FOV. Different regions within the larger, mosaiced image then have different acquisition times, each corresponding to the acquisition time of the smaller, overlapping strip used in each particular region.

Accounting for shifts in the acquisition times due to mosaicing is the critical step to establishing the relative acquisition times between pixels in the mosaiced image. To test our method of identifying the time shifts, we compare the velocities of aircraft as measured from PLC images with the velocities reported by onboard ADS-B transponders and archived by the OpenSky Network (OpenSky Network 2024).

In push broom scanning, the overlapping single-zone images are aligned with their long axes perpendicular to the satellite orbit. The effects of mosaicing on the apparent velocities of moving objects are most pronounced in tracks that are approximately aligned with the satellite orbit. PLC satellites are in descending, sun-synchronous orbits with an orbital path just over 10° east of north. Therefore, north-south aircraft trajectories are more likely to cross mosaicing boundaries than east-west trajectories. Flight paths of aircraft on close-approach or departure at the Dallas-Fort Worth International airport (DFW) are aligned with the north-south orientation of the major runways. In addition DFW is one of the busiest in the world, with a high density of aircraft in the immediate airspace. We selected the images in PLC scene ID 20220725_161216_34_242b to test our method.

2.2. *Aircraft positions*

Moving objects can be isolated within a static background by differencing pairs of images acquired at different times. In the differenced image, a moving object appears as a positive-negative pair against a suppressed background (figure 1). In push broom scanning, the images acquired at different times are also in different spectral bands; therefore, better background suppression is achieved by differencing spectral bands that are adjacent in wavelength.

We determine the locations of the aircraft in the eight spectral bands by template matching. The template is created from the average of the images of the aircraft in bands 0 and 1, both in blue visible light, because the aircraft tend to be brighter in the shorter wavelengths. The positions of the aircraft are then determined from the minimum of the summed absolute difference between the template and the seven band-differenced images (figures 2 - 5). The aircraft locations in each spectral band are then arranged in the order of the acquisition time that corresponds to the spatial order of the spectral bands on the filter that is in front of the sensor.

2.3. *Time delays between positions*

To estimate the velocities, we require the corresponding relative acquisition times of the pixels at the aircraft positions in each spectral band. It is possible to estimate the relative acquisition times from the spacings of the positions themselves with the assumption that the aircraft is traveling at a constant velocity. The method is explained in Keto & Watters (2023, 2024).

The method takes advantage of necessities imposed by the push broom scanning technique for image acquisition. Any pixel in the larger, mosaiced image may be derived from any one of the partially overlapping single-band image strips that are sequential in time. To allow for overlap, the time between camera exposures must be shorter than the time required for the footprint of a strip in a single spectral band to advance across its own width. To minimize the

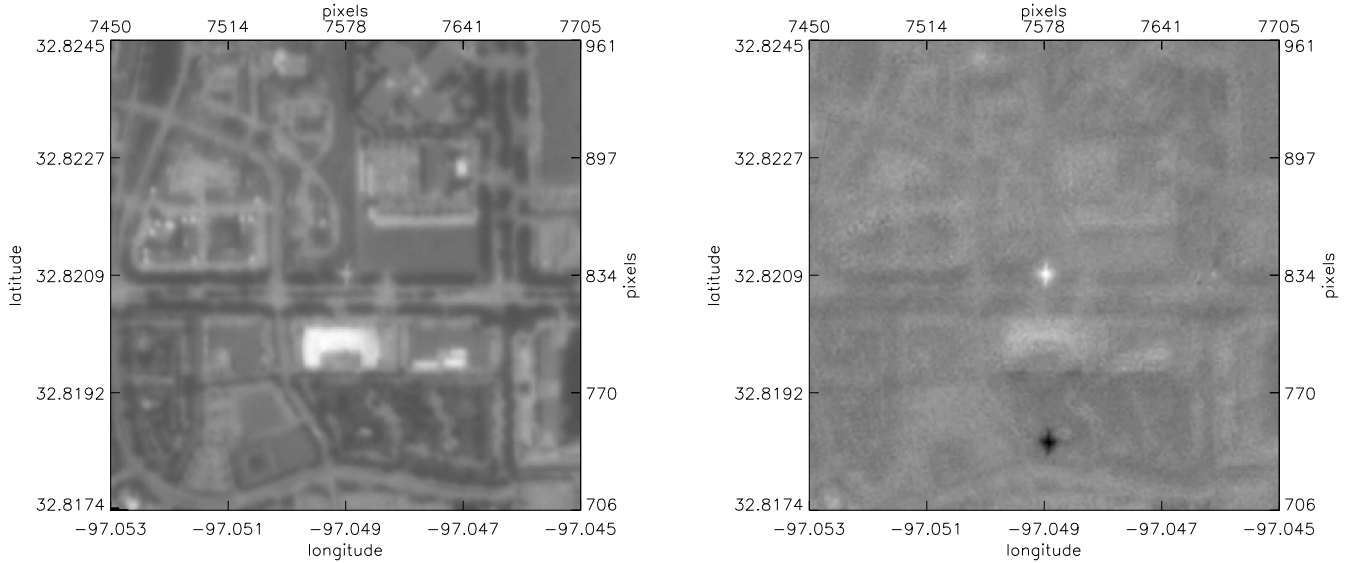


Figure 1. Aircraft in Planet Labs Corporation (PLC) scene ID 20220725_161216_34_242b. The *left* panel shows the aircraft in the center of the image in a single spectral band (0 blue). The *right* panel shows that the aircraft is more easily detectable in the difference of two bands (0-1). The subtraction causes the aircraft in band 1 to appear as a negative image. The difference in position is caused the time delay between the images in the two spectral bands. The non-moving features are suppressed by the differencing although not entirely because the features have different brightnesses in the two spectral bands. This particular aircraft is identified as track F in table 2.2.

Table 1. Pixel coordinates of airplanes along tracks A-H in the 8 spectral bands

band ¹	1		5		2		3		4		6		7 ²		0	
nm ³	465-515		650-680		513-549		547-583		600-620		697-713		845-885		431-452	
ID	x	y	x	y	x	y	x	y	x	y	x	y	x	y	x	y
A	92	2235	95	2274	97	2301	99	2327	101	2353	104	2379	108	2432
B	3196	3263	3180	3308	3164	3353	3149	3398	3133	3443	3117	3487	3086	3577
C	3785	4872	3786	4905	3787	4926	3788	4948	3789	4969	3790	4990	3792	5034
D	7411	5421	7411	5413	7412	5405	7412	5394	7412	5383	7413	5359
E	7574	2678	7574	2668	7575	2653	7576	2643	7577	2633	7579	2624	7579	2599
F	7579	835	7580	818	7580	781	7581	744
G	8246	883	8247	870	8247	851	8248	838	8248	825	8248	813	8249	787
H	8807	6120	8808	6112	8808	6104	8808	6095	8808	6087	8809	6080	8809	6059

¹ Spectral bands ordered by relative acquisition time.

² Ellipses indicate that the location could not be determined because of low S/N.

³ Spectral bandpass in nm.

quantity of data, the time between exposures should be as long as possible. For simplicity, the time between exposures may be asynchronous with the crossing time of the single-band image strips. Also for simplicity, the camera may be operating at a constant frame rate resulting in a constant time between exposures.

These requirements result in the following equation for the apparent velocity in the direction of the satellite orbit (Keto & Watters 2023, 2024),

$$v_i = \frac{\Delta p_i}{\Delta t_{band} + \alpha_i \Delta t_{camera}} \quad (1)$$

where $\Delta p_i = p_i(x, y) - p_{i+1}(x, y)$ is the distance between the locations of the object in two spectral bands, i and $i + 1$. The variable α_i can take one of three values, $-1, 0, +1$, Δt_{camera} is the time between exposures, and Δt_{band} is the time required for the footprint of one single-band image strip to cross over another. This crossing time depends on the orbital velocity of the satellite and the width of the footprint (Keto & Watters 2023, equation 1). The set of eight positions, one for each spectral band, results in eight equations for eight unknowns, α_i , and also a ninth unknown, the time between exposures, Δt_{camera} . While the set of equations appears underdetermined, the quantization of α_i represents additional information that allows a solution in two steps. First, assuming a reasonable time between exposures just smaller than half the crossing time of the smaller, single-band images, we solve for the eight variables, a_i , to minimize the deviation from constant apparent velocity. A good starting estimate is $\Delta t_{camera} = 0.184 \pm 0.007$ derived from observations of high altitude balloons Keto & Watters (2024). Second, from the equations with non-zero α_i , we solve for Δt_{camera} . This value must be the same for all the tracks in an image.

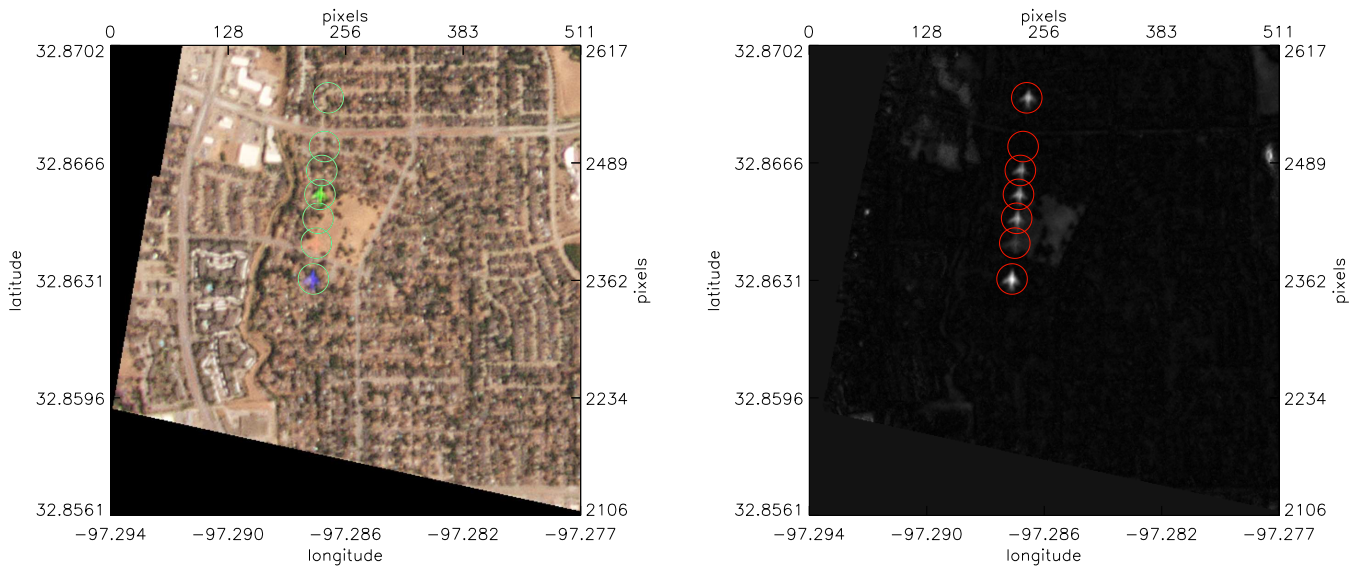


Figure 2. Track A in table 2.2. The circles show the locations of an aircraft identified from the individual spectral bands over a visual image (*left*) and over the sum of the absolute value of the seven differenced images (*right*). There is no circle for the NIR band because the signal-to-noise is too low to allow for precise localization. The location in the NIR band is between the two locations at the head of the track (top of the image). The spacing between the bottom two locations is longer than the others, not counting the gap due to the missing NIR location. This longer spacing is due to a shift in the mosaicing pattern that adds a time delay between exposures of the camera, Δt_{camera} , to the time delay equal to the crossing time, Δt_{band} , of one of the single-band image strips that are combined into a larger single-band image.

3. RESULTS

Table 2 shows the solutions for α_i that result from the minimization of the standard deviation of the apparent velocities of the segments of each aircraft track given by equation 1. Missing values indicate that the the signal-to-noise of the template match is too low for a reliable determination of the position in one or more spectral bands. In this case, the value of α_i applies to the segment between valid positions. For example, four out of the eight positions of track F have good position measurements, so there are three segments along the track. Then α_0 applies to the segment between the positions measured in spectral bands 1-5. The second value, α_1 applies to the segment between the positions in spectral bands 5-4. The last value, α_4 applies to the segment measured between bands 4-0.

The best estimate of the time between camera exposures is 0.179 ± 0.007 s derived from the seven tracks, A and C-H. Because $\alpha_i = 0$ for all segments of track B, the velocities for this track do not depend on Δt_{camera} .

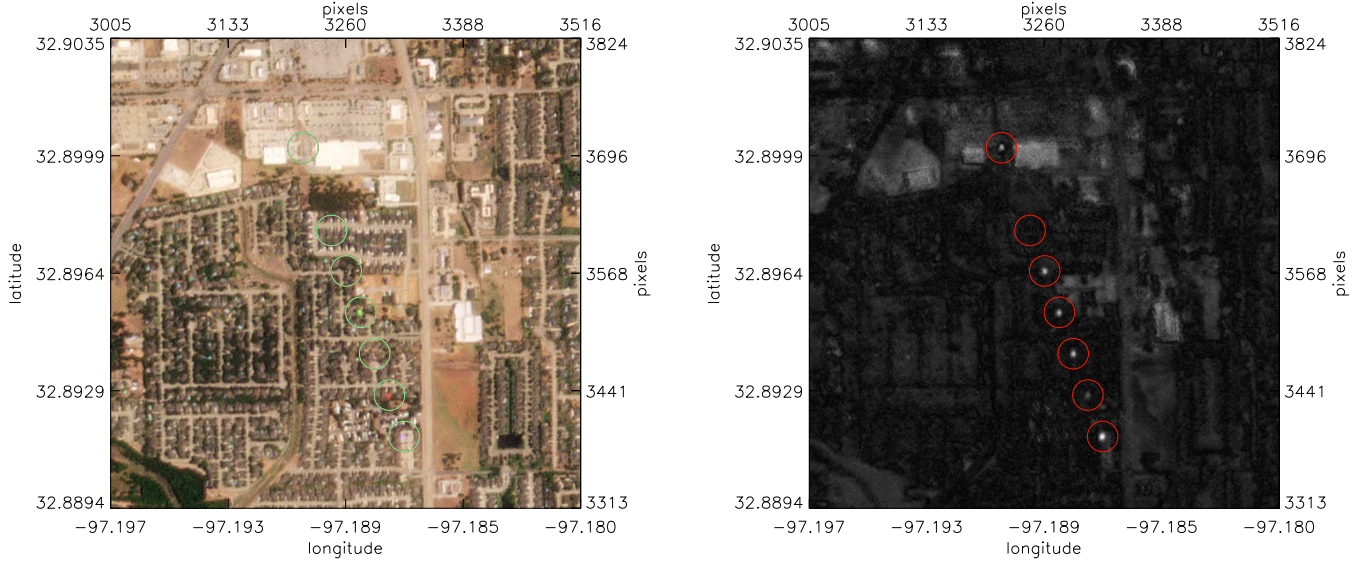


Figure 3. Track B in table 2.2 in the same format as figure 2. In this case the identified locations are all equally spaced. The gap between the positions at the head of the track (top of the figure) is caused by the missing NIR location. The length of the segment with this gap is exactly twice the length of the other segments.

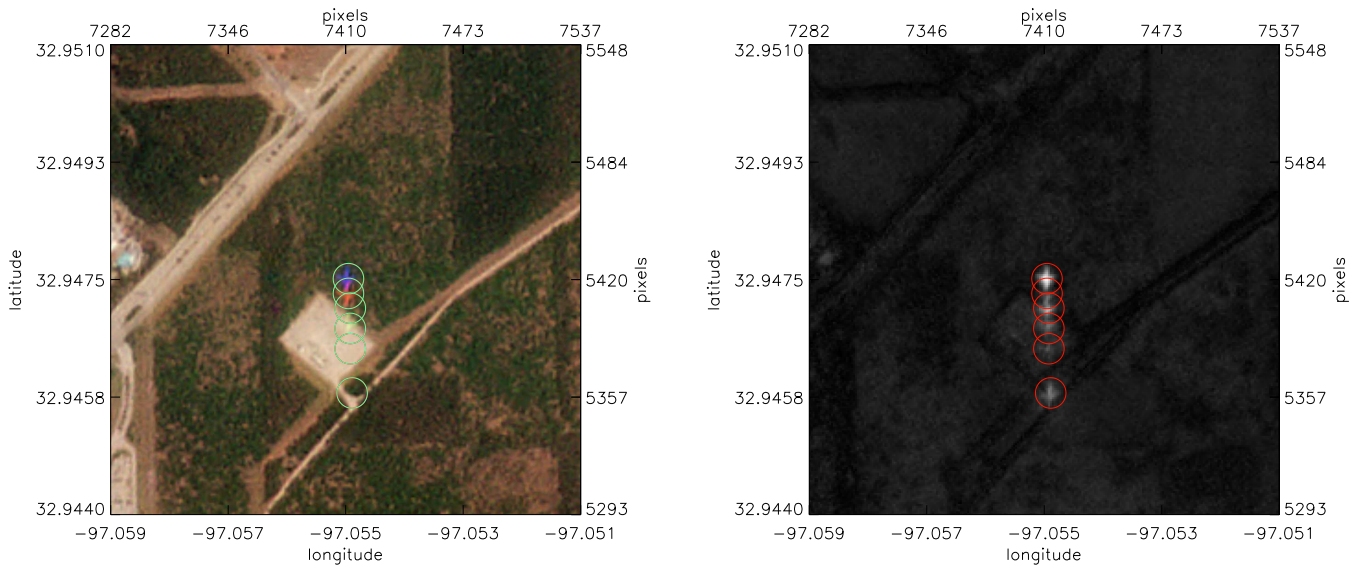


Figure 4. Track D in table 2.2 in the same format as figure 2. In this case, six positions are shown because one position, in addition to the NIR, is missing due to low signal-to-noise caused by confusion with the bright background within the track. The NIR position would be between the two positions at the head of the track toward the bottom of the figure. The first two segments at the beginning of the track are shorter than the next two, each of which has an additional time delay equal to the time between exposures of the camera.

Table 3. True velocity vs. altitude for track F

Altitude ^a	true velocity
(m)	(m s ⁻¹)
0	91.1
305	95.5
610	99.9
914	104.3
1524	113.1
3048	135.4
4572	158.0
6096	180.8
9144	226.8
12497	278.2
15240	320.8

^aAbove ground level (AGL) = aircraft geo-altitude - altitude of DFW.

in the parameters of a two-line element (TLE) model for the satellite orbit published daily by PLC. The ambiguity between the altitude and the true velocity results in a family of solutions for the true velocity depending on altitude and apparent velocity. Table 3 shows an example of the true velocity as a function of altitude for track F. In this case, the altitude velocity increases with altitude because the aircraft is traveling south, close to the opposite direction of the altitude velocity, and the true velocity therefore increases with altitude to maintain the apparent velocity.

Table 4 and figure 6 compare the values for the true velocities of aircraft determined from the PLC images with the velocities transmitted from the aircraft by their onboard ADS-B transponders. The true velocity is calculated from the apparent velocity for the altitude indicated by the ADS-B data. In figure 6, the estimated errors for the velocities derived from the PLC images are 3σ where σ is the standard deviation of the velocities calculated for all segments of the track.

The errors for the altitude (geo-altitude) and velocity from the ADS-B data are derived from onboard GPS data and assumed negligible in this calculation. The ADS-B data indicate a nearly constant velocity for all aircraft over a 6 s window around the 3.2 s duration required for the satellite to image all eight bands. Although some of the aircraft are climbing or descending, the changes in the altitude velocity due to changes in the altitude over a 3.2 s track correspond to a negligible difference in the calculated true velocity of less than 1 m s^{-1} .

The velocities derived from the PLC images depend directly on the crossing time, Δt_{band} , that depends on the orbital velocity and the width of the footprint of one single-band image strip (Keto & Watters 2023, equation 1). In Keto & Watters (2023) we assumed a width of 663 pixels for a single band image strip. This results in velocities from the PLC images that are systematically 3% lower than the ADS-B velocities indicating that the camera is using 97% of the assumed sensor size of 8880×5304 . The velocities in table 4 and figure 6 are calculated with a width of 643 pixels for a single band image strip.

Table 4. Comparison of velocities from ADS-B and PLC images

Track	altitude (m)	ADS velocity (m/s)	PL velocity (m/s)	std. dev. ^a (m/s)
A	2985	178	177.8	2.8
B	12731	247	256.0	2.0
C	2977	138	137.7	3.5
E	158	74	67.4	3.3
F	400	90	88.9	3.0
G	760	102	102.0	4.2
H	653	115	117.0	3.8
I	371	77	73.4	5.7

^aThe standard deviation is a measure of the accuracy of the velocity calculated from the PLC images, specifically the differences in the velocities of the segments of the track segments.

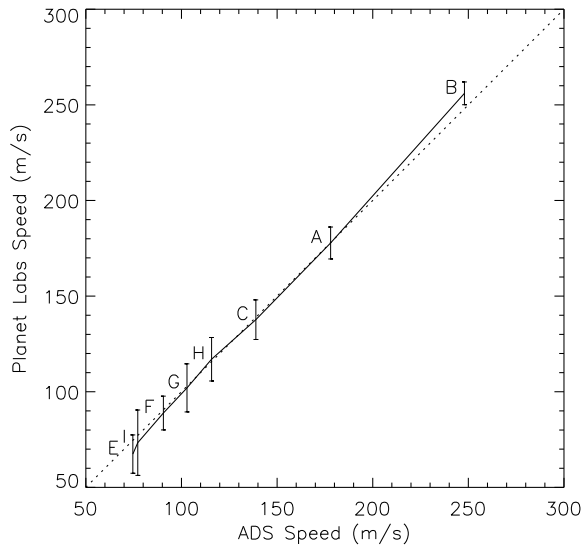


Figure 6. Comparison of velocity of aircraft as calculated from the PLC images versus the velocity broadcast from onboard ADS-B transponders. The vertical error bars are 3σ where σ is the standard deviation of the velocities for each segment.

4. DISCUSSION

Our method for determining the relative acquisition times within regions of a multi-spectral image relies on an assumption of the constant velocity of a moving object to identify time shifts introduced by PLC’s mosaicing procedure to produce the images in their archive. This assumption is not strictly necessary and the method can be applied to objects that accelerate within the ~ 3.2 s time required to observe a scene in all eight spectral bands. This follows because the necessities imposed by push broom scanning, described in §2.3, restrict the variable α_i in equation 1 to discrete values of $-1, 0, +1$. Therefore, differences in the apparent velocities along a track that are due to acceleration

are generally incompatible with time shifts introduced by mosaicing. Accelerating objects can be recognized by an uncharacteristically large standard deviation of the apparent velocities of the track segments. Acceleration necessarily complicates the determination of the velocity. Our future research will explore the generalization of the method to analyze accelerating objects and define any limitations of the method.

Conventional aircraft are not generally expected to exhibit significant acceleration within 3.2 s. Objects with uncharacteristic flight patterns such as sudden acceleration would be of interest in our research with the Galileo Project at Harvard University whose goal is to collect scientific quality data that may be useful in the search for objects of extraterrestrial origin (<https://projects.iq.harvard.edu/galileo/home>).

5. CONCLUSIONS

Our study demonstrates a novel method for detecting and analyzing the velocities of moving objects using multi-spectral images from push broom scanning satellites. By estimating the relative acquisition times between different spectral bands, we can accurately determine the velocities of moving objects, such as aircraft, even in the absence of precise timestamp information. Our study repurposes single-image survey data from Planet Labs Corporation SuperDove satellites for the quantitative analysis of dynamic phenomena with characteristic time scales on the order of seconds.

Key findings from our study include:

1. Method Validation: By comparing the velocities of aircraft derived from satellite images with those reported by onboard ADS-B transponders, we verify the accuracy and reliability of our method. The close agreement between the two sets of velocities confirms the efficacy of our approach.
2. Commercial Satellite Data Utilization: Despite the challenges posed by proprietary restrictions on commercial satellite data, our study demonstrates the potential for scientific research using these data sources. By developing techniques to infer missing temporal details, we can enhance the utility of commercial satellite imagery.

Our work highlights the transformative impact of the commercialization of space on Earth observation. The high spatial resolution and frequent revisit rates of Planet Labs Corporation satellites offer unprecedented opportunities for detailed and timely observations of dynamic phenomena. However, the full scientific potential of these data can only be realized by addressing challenges related to data access and completeness.

6. ACKNOWLEDGMENTS

Funding for access to Planet Labs data was provided by the Galileo Project at Harvard University. We acknowledge Planet Labs Corp. for technical support. We thank Dr. Matthew Szenher for help with the ADS-B data.

REFERENCES

- Chen, Y., Qin, R., Zhang, G., & Albanwan, H. 2021, *Remote Sensing*, 13, 208, doi: [10.3390/rs13020208](https://doi.org/10.3390/rs13020208)
- Drouyer, S., de Franchis, C., & Philipp. 2019, in *2019 IEEE International Geoscience and Remote Sensing Symposium (IEEE Geoscience and Remote Sensing Society)*
- Easson, G., DeLozier, S., & Momm, H. 2010, *Remote Sensing*, 2, 1331
- Etaya, M., Sakata, T., Shimoda, H., & Matsumae, Y. 2004, *Journal of the Remote Sensing Society of Japan*, 24, 357
- Heiselberg, H. 2019, *Sensors*, 19, 2873
- Heiselberg, P., & Heiselberg, H. 2021, *Remote Sensing*, 13, 3016
- Keto, E., & Watters, W. A. 2023, *Journal of Astronomical Instrumentation*, 12, 2340007, doi: [10.1142/S225117172340007X](https://doi.org/10.1142/S225117172340007X)
- . 2024, *Journal of Astronomical Instrumentation*, submitted
- OpenSky Network. 2024, Open Air Traffic Data for Research, <https://opensky-network.org>, OpenSky Network
- Planet Labs Corporation. 2021, Understanding PlanetScope Instruments, <https://developers.planet.com/docs/apis/data/sensors/>, Planet Labs Corporation
- van Etten, A. 2024, Vehicle Vectors and Traffic Patterns from Planet Imagery, <https://arxiv.org/abs/2406.06320>, arXiv, Cornell University, doi: [10.48550/arXiv.2406.06320](https://doi.org/10.48550/arXiv.2406.06320)